PHYSICAL REVIEW B **68**, 094417 (2003)

Critical control of competition between metallic ferromagnetism and charge/orbital correlation in single crystals of perovskite manganites

Y. Tomioka,[1] Y. Okimoto,[1] J. H. Jung,[2] R. Kumai,[1] and Y. Tokura[1–3]
[1]*Correlated Electron Research Center (CERC), National Institute of Advanced Industrial Science and Technology (AIST), Tsukuba 305-8562, Japan*
[2]*Spin Superstructure Project (SSS), ERATO, Japan Science and Technology Corporation (JST), Tsukuba 305-8562, Japan*
[3]*Department of Applied Physics, University of Tokyo, Tokyo 113-8656, Japan*

(Received 21 April 2003; published 17 September 2003)

The transition between a ferromagnetic metal and an insulator with short-range charge/orbital correlation has been investigated for the manganites $R_{0.55}Sr_{0.45}MnO_3$ [$R=$Sm, Eu, Gd, and $Sm_{1-y}Gd_y$ ($0\leqslant y\leqslant 1$)]. The phase diagram as a function of the averaged radius of perovskite *A*-site cations is entirely modified from the prototypical bicritical phase diagram, e.g., for $Pr_{0.55}(Ca_{1-y}Sr_y)_{0.45}MnO_3$ with the competition between the ferromagnetic metal and charge/orbital-ordered insulator. Larger randomness via the local lattice distortion in $R_{0.55}Sr_{0.45}MnO_3$ enhances the phase fluctuation between ferromagnetic metal and charge/orbital-ordered insulator and suppresses their long-range orders.

DOI: 10.1103/PhysRevB.68.094417 PACS number(s): 71.27.+a, 71.30.+h, 75.30.Kz

I. INTRODUCTION

Manganese oxides with perovskite structure have been attracting great interest since they show a variety of intriguing phenomena due to a unique coupling among spin, charge, and orbital degrees of freedom of $3d$ electrons.[1] One such example is colossal magnetoresistance (CMR). The magnitude of CMR cannot be described by the magnetic scattering mechanism alone, and it has been suggested that the importance of an electron-lattice coupling related with Jahn-Teller distortion plays an important role.[2,3] The lattice effects on CMR have been studied experimentally on $R_{0.7}A_{0.3}MnO_3$ (R^{3+} and A^{2+} being usually rare-earth elements and alkaline-earth-metal elements, respectively).[4] In $(La_{1-y}Pr_y)_{0.7}Ca_{0.3}MnO_3$,[4] for example, the ferromagnetic metal (FM) at $y=0$ changes to an insulator at $y=1$ while keeping the hole-doping level constant, and the magnitude of the magnetoresistance (MR) is enormously enhanced as y increases, or the lattice distortion increases. In $R_{1-x}A_xMnO_3$, a decrease of the averaged radius of R^{3+} and A^{2+} leads to an increase of the tilting of MnO_6 octahedra, which causes the reduction of hybridization between Mn $3d$ e_g and O $2p$ states, i.e., the effective one-electron bandwidth (W).[5] In such a reduced-W case, the FM due to the double exchange mechanism[6,7] suffers from other competing instabilities, such as the electron-lattice coupling (Jahn-Teller distortion), antiferromagnetic interaction between local t_{2g} spins, charge/orbital ordering (CO/OO), and so on.[8] Under such a competition, the removal of the antiferromagnetic interaction originating from the charge/orbital correlation by magnetic fields seems to cause CMR.[8,9]

Another noteworthy aspect is an electronic phase separation as a generic feature of the systems with disorder.[10–12] For the electronic phases competing with each other, e.g., the FM and CO/OO, the relative stability as well as the fluctuation of the respective phases is drastically affected by quenched disorder, e.g., the random chemical replacement at the perovskite *A* sites. However, most of the previous works reporting the phase separation have been done using the polycrystalline sintered specimens, in which the grain boundaries seem to be more effective than the chemical substitution alone and mask the dramatic feature arising from the quenched disorder inherent to the doped perovskite.

In this paper, we investigate the metal-insulator phenomena in single crystals of $R_{0.55}Sr_{0.45}MnO_3$ [$R=$Sm, Eu, Gd, and $Sm_{1-y}Gd_y$ ($0\leqslant y\leqslant 1$)]. A systematic study of $(Sm_{1-y}Gd_y)_{0.55}Sr_{0.45}MnO_3$ indicates that the FM is kept up to $y\sim 0.5$ (corresponding to $R=$Eu) with a reduced T_C of $\sim$50 K, while it changes to a spin-glass- (SG) like insulator for $y\geqslant 0.6$. We demonstrate the *R*- or *y*-dependent competing features between a FM and a paramagnetic or SG-like insulator[13,14] with short-range charge/orbital correlation. No macroscopic phase separation is discerned when high-quality single-crystal specimens are used. Near the metal-insulator phase boundary, the CMR and field-induced insulator-to-metal transition are turned into the most conspicuous ones.

II. EXPERIMENTAL PROCEDURES

Single crystals of $R_{0.55}Sr_{0.45}MnO_3$ [$R=$Sm, Eu, Gd, and $Sm_{1-y}Gd_y$ ($0\leqslant y\leqslant 1$)] were prepared by the floating zone method. The mixed powders of R_2O_3, $SrCO_3$, and Mn_3O_4 with a prescribed ratio were calcined at 1100 °C for 12–24 h in air. The powders were pulverized and again sintered in the same condition. Then the powders were pressed into a rod 4 mm in diameter and about 70 mm in length, and the rod was fired at 1200–1300 °C for 24 h in air. The crystal was grown in an oxygen atmosphere by rotating the feed and seed rods in opposite directions. The growth rate was set 10–20 mm/h. The obtained crystals were pulverized and checked by a powder x-ray diffraction (XRD) with Cu $K\alpha$ radiation (MXP18 AHF,[22] MAC Science Co, Ltd). The diffraction pattern was collected by the $\theta/2\theta$ step scanning method in the range $15°\leqslant 2\theta\leqslant 110°$. Reitveld refinement of the XRD pattern indicated that the obtained crystal is a single phase, and that the crystal structure is orthorhombic *Pbnm* with the re-

TABLE I. The analyzed cation ratio, lattice parameters, and transition temperatures of $(\mathrm{Sm}_{1-y}\mathrm{Gd}_y)_{1-x}\mathrm{Sr}_x\mathrm{MnO}_3$ prepared by the floating zone method with the prescribed compositions, $x=0.45$ and $y=0-1$.

y (nominal)	x Sr/(Sm+Gd+Sr)[a]	y Gd/(Sm+Gd)[a]	Lattice parameters, a_0, b_0, and c_0 (Å)	T_C,[b] T_G[c] (K)
0	0.451	0	$a_0=5.4401$, $b_0=5.4253$, $c_0=7.6556$	134.8[b]
0.1	0.449	0.0967	$a_0=5.4382$, $b_0=5.4263$, $c_0=7.6540$	127.3[b]
0.3	0.446	0.301	$a_0=5.4345$, $b_0=5.4273$, $c_0=7.6541$	94.8[b]
0.4	0.449	0.400	$a_0=5.4326$, $b_0=5.4258$, $c_0=7.6518$	83.9[b]
0.5	0.444	0.504	$a_0=5.4306$, $b_0=5.4254$, $c_0=7.6510$	64.2[b]
0.6	0.447	0.599	$a_0=5.4248$, $b_0=5.4293$, $c_0=7.6468$	49.1[c]
0.7	0.434	0.707	$a_0=5.4246$, $b_0=5.4292$, $c_0=4.6457$	44.7[c]
1	0.450	1	$a_0=5.4183$, $b_0=5.4316$, $c_0=7.6434$	44.0[c]

[a] The cation ratio was determined by the inductively coupled plasma (ICP) spectroscopy.

[b] The averaged value of the transition temperatures in the cooling and warming runs.

[c] The temperature at which a cusp structure appears in the ZFC magnetization at 100 Oe.

lation $a_0 \sim b_0 \sim c_0/\sqrt{2} \sim \sqrt{2}a_p$, where a_p is the lattice parameter of the pseudocubic setting. The cation ratio of the obtained crystals was also checked by the inductively coupled plasma (ICP) spectroscopy and found to nicely coincide with the prescribed one. The analyzed cation ratio, lattice parameters, and the transition temperatures for several crystals of $(\mathrm{Sm}_{1-y}\mathrm{Gd}_y)_{0.55}\mathrm{Sr}_{0.45}\mathrm{MnO}_3$ are listed in Table I.

Magnetization was measured by a SQUID magnetometer (MPMS, Quantum Design Inc.). The ac susceptibility was also measured with varying the frequency from 0.5 to 10 kHz. The amplitude of the ac excitation magnetic field was 10 Oe. Resistivity in magnetic fields was measured in a cryostat equipped with a superconducting magnet up to 7 T. The electrodes for the resistivity measurement were made by a gold paste.

A single crystal x-ray diffraction was performed using an imaging plate system with monochromated Mo $K\alpha$ radiation. A crystal was mounted on a goniometer with a (100) plane of the pseudocubic setting almost perpendicular to a beam axis. The temperature was changed down to around 35 K with use of a closed cycle helium refrigerator. To measure the Raman scattering, we prepared a cleaved surface and focused an incident light from a He-Ne laser ($\lambda=6328$ Å) on the sample. A magnetic field up to 5 T was applied with a superconducting magnet. The scattered light in the backscattering configuration was collected through a notch filter and dispersed by a monochromator equipped with a cooled charge-coupled device detector.

III. RESULTS AND DISCUSSION

A. An overview of an electronic phase diagram

Figure 1 shows the temperature profiles of (a) intensity of x-ray diffuse scattering around (220) in the orthorhombic *Pbnm* setting [corresponding to the (020) reflection in the pseudocubic setting[1]] for $R_{0.55}\mathrm{Sr}_{0.45}\mathrm{MnO}_3$ ($R=$ Sm, Eu, and Gd), (b) intensity of the Raman phonon mode around 490 cm^{-1} for $(\mathrm{Sm}_{1-y}\mathrm{Gd}_y)_{0.55}\mathrm{Sr}_{0.45}\mathrm{MnO}_3$ ($y=0$, 0.5, and 0.7), and (c) resistivity for $R_{0.55}\mathrm{Sr}_{0.45}\mathrm{MnO}_3$ ($R=$ Nd, Sm, Eu, and Gd) as well as $(\mathrm{Sm}_{1-y}\mathrm{Gd}_y)_{0.55}\mathrm{Sr}_{0.45}\mathrm{MnO}_3$ ($y=0.5$ and 0.7). The diffuse scattering intensity [Fig. 1(a)] and the Raman intensity [Fig. 1(b)] both represent the charge/orbital correlation, as described later. In Fig. 1(c), an anomaly in resistivity is seen at ~280 K ($=T_C$) for $R=$ Nd, while it is lowered to ~130 K for $R=$ Sm. For $R=$ Eu, T_C is further lowered to ~50 K with a change in resistivity by more than seven orders of magnitude. For $R=$ Gd, the resistivity is no more metallic down to the lowest temperature. For an alloying system of $(\mathrm{Sm}_{1-y}\mathrm{Gd}_y)_{0.55}\mathrm{Sr}_{0.45}\mathrm{MnO}_3$, the FM is seen as the ground state at $0 \leqslant y \leqslant 0.5$, while an insulator at $0.6 \leqslant y \leqslant 1$. In Fig. 1(c), the temperature profiles of resistivity for $(\mathrm{Sm}_{1-y}\mathrm{Gd}_y)_{0.55}\mathrm{Sr}_{0.45}\mathrm{MnO}_3$ ($y=0.5$ and 0.7) are also shown in comparison with those of $\mathrm{Eu}_{0.55}\mathrm{Sr}_{0.45}\mathrm{MnO}_3$ and $\mathrm{Gd}_{0.55}\mathrm{Sr}_{0.45}\mathrm{MnO}_3$, respectively, whose resistive (and other) behaviors go almost parallel.

In the CO/OO with $x=1/2$ at $T<T_{\mathrm{CO}}$, superlattice diffractions, e.g., $(2\frac{3}{2}0)$ or $(2\frac{5}{2}0)$ in the orthorhombic *Pbnm* setting,[16] are formed due to the e_g-orbital ordering on the Mn^{3+} sublattice.[17,18] Even above T_{CO}, the diffuse scatterings are visible as a sign of the charge/orbital correlation in a short range.[19–21] In this paper, the intensity of the diffuse scattering at (2 1.7 0) has been estimated by fitting the profile of $(2+\Delta h\ 1.7\ 0)$ [$-0.5 \leqslant \Delta h \leqslant 0.5$, inset of Fig. 1(a)] with a Gaussian form. In Fig. 1(a), for $R=$ Sm and Eu, the intensity of diffuse scattering increases as temperature approaches

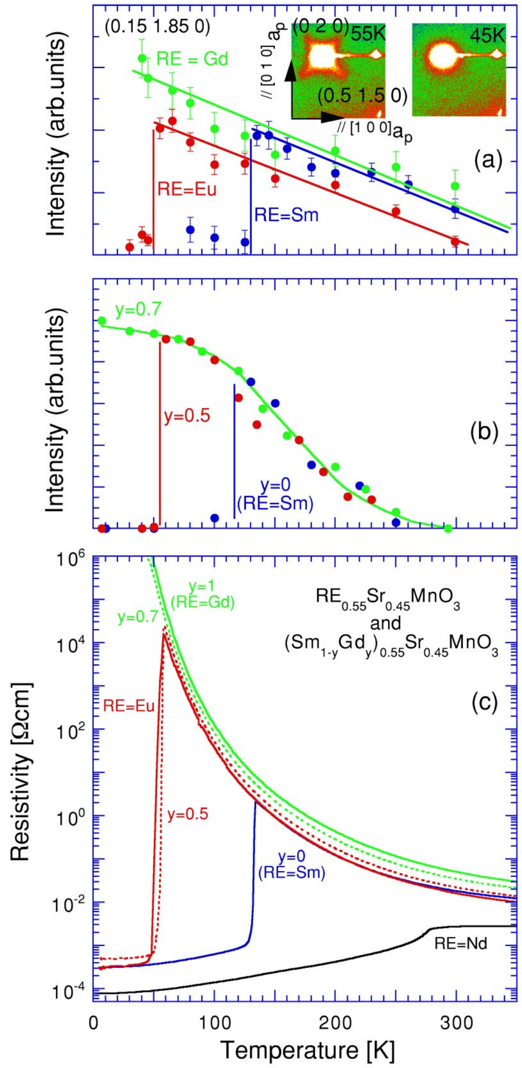

FIG. 1. (Color online) Temperature profiles of (a) intensity of x-ray diffuse scattering around (020) diffraction for $R_{0.55}Sr_{0.45}MnO_3$ ($R=$Sm, Eu, and Gd), (b) intensity of Raman phonon mode around 490 cm^{-1} (see Fig. 3) for $(Sm_{1-y}Gd_y)_{0.55}Sr_{0.45}MnO_3$ ($y=0$, 0.5, and 0.7), and (c) resistivity in cooling runs for the crystals of $R_{0.55}Sr_{0.45}MnO_3$ ($R=$Nd, Sm, Eu, and Gd) (solid line) as well as $(Sm_{1-y}Gd_y)_{0.55}Sr_{0.45}MnO_3$ ($y=0.5$ and 0.7) (dotted line). The solid line in Figs. 1(a) and 1(b) is the guide for the eye. Inset of (a) shows x-ray diffuse scattering around (020) reflection for $Eu_{0.55}Sr_{0.45}MnO_3$ taken at 55 and 45 K. The intensity of the diffuse scattering at (0.15 1.85 0) has been estimated by fitting the profile of $(0.15+\delta\, 1.85+\delta\, 0)$ $(-0.25\leqslant\delta\leqslant 0.25)$ with Gaussian form, and it has been normalized by an intensity of (110) reflection. The reflections are indexed in the pseudocubic setting. The reflection at the right side of (020) is due to the twinning of the crystal.

T_C, but it is suddenly decreased at T_C, which is in accord with the resistive transition shown in Fig. 1(c). For $R=$Gd, on the other hand, the diffuse scattering intensity is found to persist to the lowest temperature. The intensities of the Raman phonon modes indicating the charge/orbital correlation [*vide infra*, Fig. 1(b)] show features very similar to the x-ray diffuse scattering.

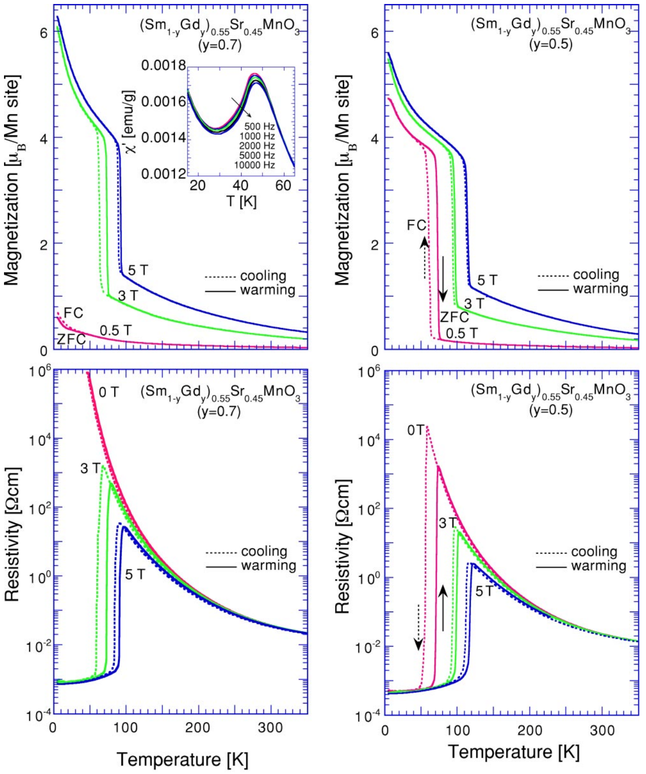

FIG. 2. (Color online) Temperature profiles of magnetization (upper) as well as resistivity (lower) in magnetic fields for the crystals of $y=0.5$ (right) and 0.7 (left) of $(Sm_{1-y}Gd_y)_{0.55}Sr_{0.45}MnO_3$. For the magnetization measurement, the sample was first cooled to the lowest temperature at zero field, and then the magnetic field was set at 0.5 T, and the zero-field-cooled (ZFC) magnetization was measured with increasing temperature. For the cooling run, the field-cooled (FC) magnetization was subsequently measured with decreasing temperature at the same magnetic field. For the other measurements of magnetization as well as resistivity, a prescribed magnetic field was first set at the highest temperature, and the cooling and warming runs were measured. The cooling and warming runs are indicated by the dotted and solid lines, respectively. Inset shows the ac susceptibility at low temperatures for the $y=0.7$ crystal.

Figure 2 shows temperature profiles of magnetization (upper) as well as resistivity (lower) in magnetic fields for the crystals of $y=0.5$ (right) and 0.7 (left) of $(Sm_{1-y}Gd_y)_{0.55}Sr_{0.45}MnO_3$, which are located in the immediate vicinity of the metal-insulator phase boundary. As shown in the resistivity at zero field, a FM is seen as the ground state for $y=0.5$, while an insulator is seen for $y=0.7$. In the case of $y=0.7$, however, a metallic state starts to appear at 3 T and below ~50 K. As the magnetic field is intensified, the metallic state is relatively stabilized in common to the cases of $y=0.5$ and 0.7. In the both cases of $y=0.5$ and 0.7, rather discontinuous changes of magnetization as well as resistivity are observed as accompanied by thermal hysteresis, indicating the first order nature of the transition.

For $y>0.5$, a SG-like state also becomes prevailing.[13,14] The inset shows temperature profiles of ac susceptibility of the $y=0.7$ crystal, which is a typical example of the insulat-

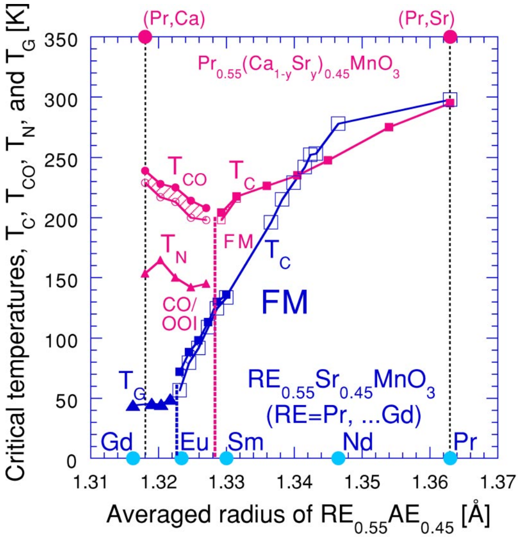

FIG. 3. (Color online) The electronic phase diagram of $R_{0.55}Sr_{0.45}MnO_3$ ($R=$Pr, Nd, Sm, Eu, and Gd) as a function of the averaged ionic radius of the A site in comparison with that of $Pr_{0.55}(Ca_{1-y}Sr_y)_{0.45}MnO_3$. For the $R_{0.55}Sr_{0.45}MnO_3$ system, the data for $(Nd_{1-y}Sm_y)_{0.55}Sr_{0.45}MnO_3$ $(0<y<1)$ and $(Sm_{1-y}Gd_y)_{0.55}Sr_{0.45}MnO_3$ $(0<y<1)$ are also indicated. The charge/orbital-ordered insulator (for $Pr_{0.55}(Ca_{1-y}Sr_y)_{0.45}MnO_3$) and ferromagnetic metal are denoted as CO/OOI and FM, respectively. The transition from (to) CO/OOI is represented by closed (open) circles, and that from (to) FM by closed (open) squares, respectively. The spin-glass (SG) transition temperature T_G (for $(Sm_{1-y}Gd_y)_{0.55}Sr_{0.45}MnO_3$ $(0.6\leqslant y\leqslant 1)$) is indicated by closed triangles. The hysteresis regions are hatched.

ing phases at $y>0.5$ in $(Sm_{1-y}Gd_y)_{0.55}Sr_{0.45}MnO_3$. As shown in the inset, cusp structures are seen around 45 K, and the susceptibility below ~45 K becomes frequency dependent. These features are characteristic of a SG state, indicating that the ground state at $y>0.5$ is a SG-like insulator.

Figure 3 shows the electronic phase diagram of the $R_{0.55}Sr_{0.45}MnO_3$ crystals as a function of the averaged radius of the A-site ions in comparison with that of $Pr_{0.55}(Ca_{1-y}Sr_y)_{0.45}MnO_3$.[15] In $R_{0.55}Sr_{0.45}MnO_3$, T_C decreases from ~280 to ~130 K as R changes from Nd to Sm.[9] In $(Sm_{1-y}Gd_y)_{0.55}Sr_{0.45}MnO_3$, it further decreases down to ~50 K at $y\sim0.5$, and then the FM is taken over by a SG-like insulator for $y\geqslant0.6$. As shown in Figs. 1(a) and 1(b), the intensities of the x-ray diffuse scattering for $R=$Gd and the Raman phonon mode at 490 cm^{-1} for $y=0.7$ seem to be saturated below ~50 K. This suggests that the charge/orbital correlation remains short-ranged down to the lowest temperature. Below T_G, therefore, neither the long-range order of FM nor CO/OO is realized. In the $Pr_{0.55}(Ca_{1-y}Sr_y)_{0.45}MnO_3$ system, by contrast, the reduction in T_C is not so remarkable as in the $R_{0.55}Sr_{0.45}MnO_3$ system. Moreover, the phase change from a FM to a CO/OO (long range) insulator is typically bicritical with $T_C=T_{CO}$ ~200 K.[13,14] That is, the phase diagram of the $R_{0.55}Sr_{0.45}MnO_3$ system is different from the bicritical feature in spite of the common hole-doping level and even when the averaged radius of the perovskite A site is taken as the common abscissa. The dramatic modification of the FM vs CO/OO phase diagrams is quite analogous to the case of the A-site order versus disorder of $R_{0.5}Ba_{0.5}MnO_3$,[23] where the perfect R/Ba ordering along the c axis alters the phase diagram of the R/Ba solid solution (similar to the present one of the R/Sr solid solution) to the typical bicritical phase diagram [similar to that of $Pr_{0.55}(Ca_{1-y}Sr_y)_{0.45}MnO_3$]. Therefore, the large modification of the phase diagram in the present case (Fig. 3) is likely to arise from the random potential affecting on the FM vs CO/OO bicritical feature. In the present case, as argued in Ref. 22, the source of the random potential may be the local lattice distortion arising from the larger mismatch of the ionic size of R(Sm, Eu, and Gd)/Sr ions than Pr/(Ca, Sr) ones.

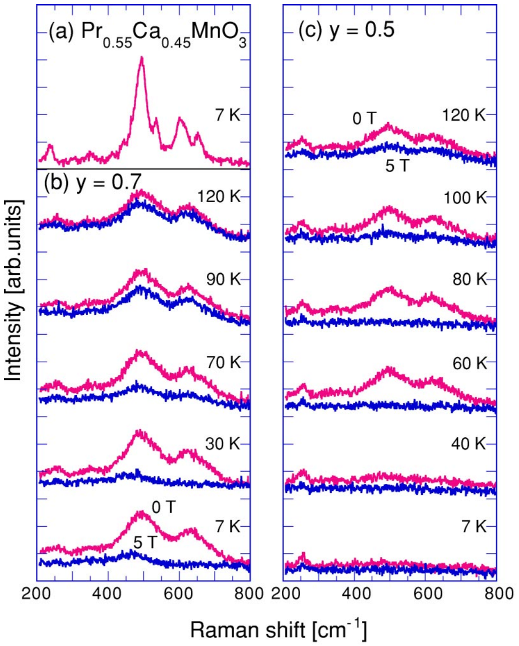

FIG. 4. (Color online) Temperature profiles of Raman phonon spectra (taken at the geometry of incident and scattered light polarizations parallel with each other) at zero field and 5 T for the crystals of $(Sm_{1-y}Gd_y)_{0.55}Sr_{0.45}MnO_3$ with (b) $y=0.7$ and (c) $y=0.5$. For comparison, the spectra of the $Pr_{0.55}Ca_{0.45}MnO_3$ crystal are also shown in (a).

B. Raman phonon spectra

Figure 4 shows the temperature profiles of the Raman phonon spectra for the crystals of (b) $y=0.7$ and (c) $y=0.5$ of $(Sm_{1-y}Gd_y)_{0.55}Sr_{0.45}MnO_3$, which were taken at zero field and 5 T in the incident and scattered light polarizations parallel with each other. For comparison, the spectra of a $Pr_{0.55}Ca_{0.45}MnO_3$ crystal with a long range CO/OO below ~220 K is also displayed in Fig. 4(a). In the spectra, two major peaks are seen at ~490 cm^{-1} (Jahn-Teller mode) and ~600 cm^{-1} (breathing mode). The both peaks have been assigned to the activated modes due to the CO/OO accompanied with collective Jahn-Teller distortion of MnO_6 octahedra.[24,25] In the case of $y=0.5$, the intensities of the phonon modes at zero field show a slight increase as the

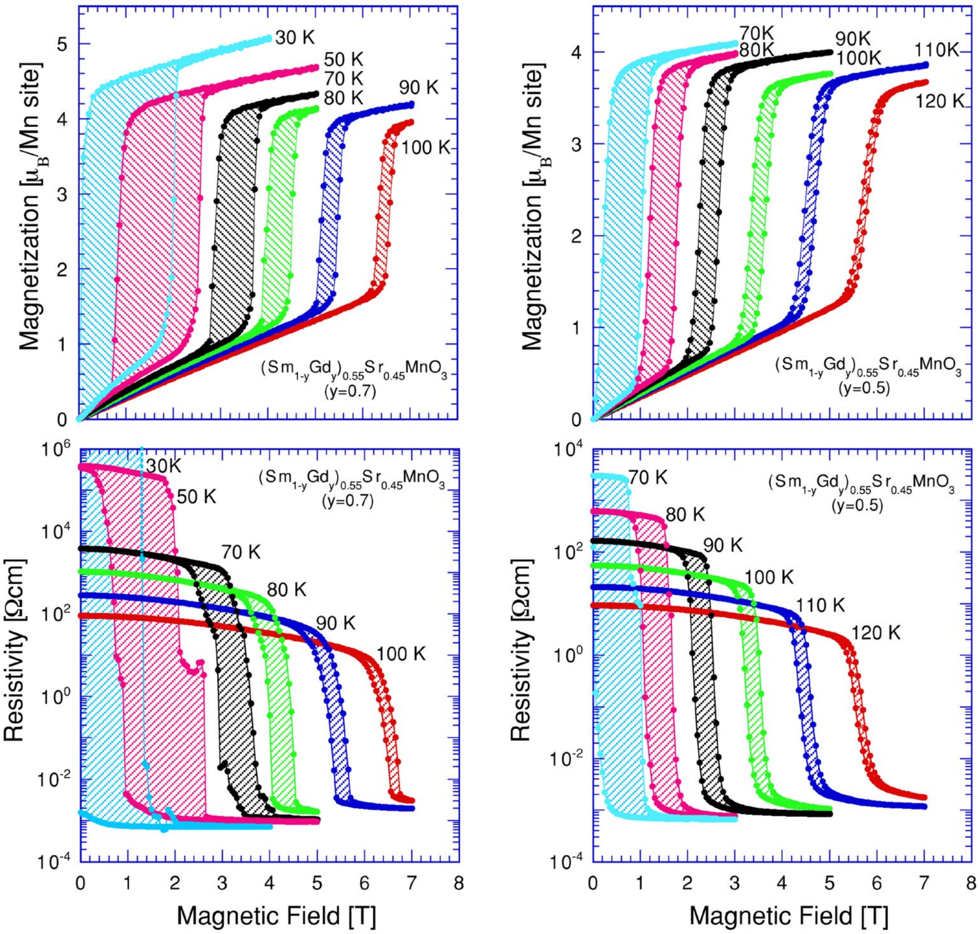

FIG. 5. (Color online) The isotherms of magnetization (upper) as well as resistivity (lower) versus external magnetic field for the crystals of $(Sm_{1-y}Gd_y)_{0.55}Sr_{0.45}MnO_3$ with $y=0.5$ (right) and $y=0.7$ (left). For the both cases, the crystals were first cooled to a prescribed temperature at zero field, and then the magnetization as well as resistivity were measured.

temperature is lowered from 120 to 60 K. Below T_C ($\sim$50 K), however, the phonon bands disappear. In the case of $y=0.7$, on the other hand, both phonon modes at zero field seem to increase in intensity with the decrease of temperature and keep finite intensities even at the lowest temperature. That is, the short-range charge/orbital correlation is removed at $T<T_C$ for $y=0.5$, while it remains down to the lowest temperature for $y=0.7$. Note that the temperature variations of the Raman mode intensity for $y=0$, 0.5, and 0.7 are closely correlated with those of the x-ray diffuse scattering intensity and resistivity as noticed in Fig. 1.

An impact of application of an external magnetic field appears also in the Raman phonon spectra. In the case of $y=0.5$, the phonon modes at $\sim$490 cm^{-1} and $\sim$600 cm^{-1} are distinctly seen at 60 and 80 K at zero field, while they disappear at 5 T. At 100 K, they are strongly suppressed at 5 T though still discernable. In the case of $y=0.7$, similarly to the case of $y=0.5$, the phonon modes are seen at 7 and 30 K at zero field, while they almost disappear at 5 T. At 70 K, they are strongly suppressed at 5 T. For the both $y=0.5$ and 0.7 crystals, the observed changes in the Raman phonon spectra by variations of temperature and magnetic fields well agree with the results in Fig. 2.

C. Variation of *T-H* phase diagrams in $(Sm_{1-y}Gd_y)_{0.55}Sr_{0.45}MnO_3$

In Fig. 5 are shown the isotherms of the magnetization (upper) as well as resistivity (lower) versus external magnetic field (H) for the crystals of $y=0.5$ (right) and 0.7 (left) of $(Sm_{1-y}Gd_y)_{0.55}Sr_{0.45}MnO_3$. In the upper panels of Fig. 5, the metamagnetic transition is seen at some critical magnetic fields accompanied with hysteresis between the field-increasing and-decreasing runs for the both crystals. In the lower panels, the resistivity drop and jump occur at the corresponding magnetic fields. In the both figures, the changes in resistivity as well as magnetization, and the widths of hysteresis are pronounced as temperature decreases. Similarly to Fig. 2, Fig. 5 indicates that a paramagnetic ($0\leqslant y\leqslant 0.5$) or a SG-like ($0.6\leqslant y\leqslant 1$) state with the charge/orbital correlation is changed to a FM by application of magnetic fields. Figure 6 shows the *T-H* phase diagrams of $(Sm_{1-y}Gd_y)_{0.55}Sr_{0.45}MnO_3$ ($0\leqslant y\leqslant 1$) crystals under the competition between a FM and a SG-like insulator with the short-range charge/orbital correlation. In Fig. 6, the critical magnetic fields have been determined by the magnetization as well as resistivity data as shown in Fig. 5. In Fig. 6, a paramagnetic state with charge/orbital correlation at $T>T_C$

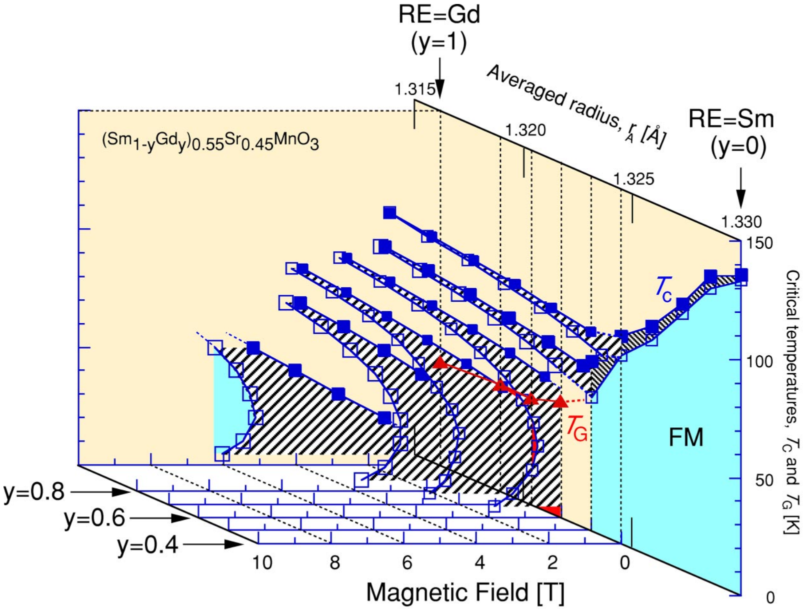

FIG. 6. (Color online) The paramagnetic or spin-glass-like insulator versus ferromagnetic metal phase diagrams for the crystals of $(\mathrm{Sm}_{1-y}\mathrm{Gd}_y)_{0.55}\mathrm{Sr}_{0.45}\mathrm{MnO}_3$ $(0 \leqslant y \leqslant 1)$. The critical fields of the transitions from (to) the ferromagnetic metal are denoted as closed (open) squares. The transitions between the paramagnetic and spin-glass-like state are denoted as closed triangles.

for $y=0.4$ and 0.5 is altered to the FM by applying magnetic fields of a few tesla, showing prototypical CMR characteristics. For $0.6 \leqslant y \leqslant 1$ where the ground state is a SG-like insulator, a paramagnetic $(T > T_G)$ or SG-like $(T < T_G)$ state at zero field is changed to a FM by application of magnetic fields, indicating the field-induced insulator to metal transition. It is also noted in Fig. 6 that the critical field for the first order transition to FM increases as y or temperature increases. The enhancement of the critical field below ~30 K is due to the supercooling effect originating from the first order nature of transition.[26]

IV. SUMMARY

In summary, we have investigated the metal-insulator phenomena in $R_{0.55}\mathrm{Sr}_{0.45}\mathrm{MnO}_3$ (R=Pr, Nd, Sm, Eu, Gd, and $\mathrm{Sm}_{1-y}\mathrm{Gd}_y$ $(0 \leqslant y \leqslant 1)$). As R changes from Sm to Eu, or more finely y increases from 0 to 0.5, T_C is reduced from ~130 K to as low as ~50 K. At $y \geqslant 0.6$ a SG-like insulator with short-range charge/orbital correlation appears. The observed behavior and phase diagram are different from a bicritical feature for $\mathrm{Pr}_{0.55}(\mathrm{Ca}_{1-y}\mathrm{Sr}_y)_{0.45}\mathrm{MnO}_3$ that shows a competition between the FM and the long-range CO/OO. Larger randomness arising from the larger mismatch of the ionic size appears to promote the phase fluctuation and to reduce the FM and CO/OO transition temperatures. In the most reduced-T_C state, the maximal CMR feature shows up with the strong CO/OO correlation down to T_C. As the bandwidth is further reduced, the charge/orbital correlation remains short-ranged, and finally frozen to a glassy state below T_G, as evidenced by the diffuse x-ray scattering and the activated broad Raman band. For $0.6 \leqslant y \leqslant 1$, a paramagnetic $(T > T_G)$, or SG-like $(T < T_G)$ insulator at zero field is changed to a ferromagnetic metal by application of an external magnetic field. The phase diagrams are demonstrated on the magnetic field versus temperature planes.

ACKNOWLEDGMENTS

The authors would like to thank S. Horiuchi for his help in x-ray diffraction experiments and N. Nagaosa for enlightening discussions. This work was partly supported by NEDO (New Energy and Industrial Technology Development Organization) of Japan.

---

[1] Y. Tokura and N. Nagaosa, Science **288**, 462 (2000).

[2] A. J. Millis, P. B. Littlewood, and B. I. Shraiman, Phys. Rev. Lett. **74**, 5144 (1995).

[3] P. Majumdar and P. B. Littlewood, Nature (London) **395**, 479 (1998).

[4] H. Y. Hwang, S.-W. Cheong, P. G. Radaelli, M. Marezio, and B. Batlogg, Phys. Rev. Lett. **75**, 914 (1995).

[5] J. B. Torrance, P. Laccore, A. I. Nazzal, E. J. Ansaldo, and Ch. Niedermayer, Phys. Rev. B **45**, 8209 (1992).

[6] P. W. Anderson and H. Hasegawa, Phys. Rev. **100**, 675 (1955).

[7] P.-G. de Gennes, Phys. Rev. **118**, 141 (1960).

[8] Y. Tokura, H. Kuwahara, Y. Moritomo, Y. Tomioka, and A. Asamitsu, Phys. Rev. Lett. **76**, 3184 (1995).

[9] Y. Tomioka, H. Kuwahara, A. Asamitsu, M. Kasai, and Y. Tokura, Appl. Phys. Lett. **70**, 3609 (1997).

[10] A. Moreo, M. Mayr, A. Feiguin, S. Yunoki, and E. Dagotto, Phys. Rev. Lett. **84**, 5568 (2000).

[11] M. Uehara, S. Mori, C. H. Chen, and S.-W. Cheong, Nature (London) **399**, 560 (1999).

[12] J. Burgy, M. Mayr, V. Martin-Mayor, A. Moreo, and E. Dagotto, Phys. Rev. Lett. **87**, 277202 (2001).

[13] T. Terai, T. Sakai, T. Kakeshita, T. Fukuda, T. Saburi, H. Kitagawa, K. Kindo, and M. Honda, Phys. Rev. B **61**, 3488 (2000).

[14] A. Sundaresan, A. Maignan, and B. Raveau, Phys. Rev. B **55**, 5596 (1997).

[15] Y. Tomioka and Y. Tokura, Phys. Rev. B **66**, 104416 (2002).

[16] Z. Jirak, S. Krupicka, Z. Simsa, M. Dlouha, and Z. Vratislav, J. Magn. Magn. Mater. **53**, 153 (1985).

[17] E. O. Wollan and W. C. Koehler, Phys. Rev. **100**, 545 (1955).

[18] J. B. Goodenough, Phys. Rev. **100**, 564 (1955).

[19] S. Shimomura, N. Wakabayashi, H. Kuwahara, and Y. Tokura, Phys. Rev. Lett. **83**, 4389 (1999).

[20] S. Shimomura, T. Tonegawa, K. Tajima, N. Wakabayashi, N. Ikeda, T. Shobu, Y. Noda, Y. Tomioka, and Y. Tokura, Phys. Rev. B **62**, 3875 (2000).

[21] Z. Jirak, F. Damay, M. Herview, C. Martin, B. Raveau, G. Andre, and F. Bouree, Phys. Rev. B **61**, 1181 (2000).

[22] L. M. Rodriguez-Martinez, and J. P. Attfield, Phys. Rev. B **63**, 024424 (2000).

[23] D. Akahoshi, M. Uchida, Y. Tomioka, T. Arima, Y. Matsui, and Y. Tokura, Phys. Rev. Lett. **90**, 177203 (2003).

[24] E. Saitoh, Y. Tomioka, T. Kimura, and Y. Tokura, J. Phys. Soc. Jpn. **69**, 2403 (2000).

[25] K. Yamamoto, T. Kimura, T. Ishikawa, T. Katsufuji, and Y. Tokura, Phys. Rev. B **61**, 14 706 (2000).

[26] H. Kuwahara, Y. Tomioka, A. Asamitsu, Y. Moritomo, and Y. Tokura, Science **270**, 961 (1995).